Journal of Neuroinflammation

RESEARCH

Open Access

Microglia-derived ADAM9 promote GHRH neurons pyroptosis by Mad2L2-JNK-caspase-1 pathway in subarachnoid hemorrhage

Jian Mao[1†], Yun Bao[1†], Fan Liu[1†], Qiyun Ye[1†], Junxiang Peng[1], Jing Nie[1], Lijun Huang[2], Yonghong Liao[3], Yiheng Xing[4], Dongyang Wu[4], Ke Wang[4], Wenfeng Feng[1], Songtao Qi[1*], Jun Pan[1*] and Binghui Qiu[1*]

Abstract

The incidence of growth hormone deficiency (GHD) after subarachnoid hemorrhage (SAH) is significantly higher than that of other neuroendocrine disorders, but the mechanism is still elusive. We used mass spectrometry to identify differentially expressed proteins in cerebrospinal fluid samples from a well-characterized cohort of patients. A total of 683 proteins were identified, including 39 upregulated proteins in the GHD group. ADAM9 was most highly associated with GHD. In vivo, ADAM9 colocalized with M1 microglia markers, GH and cognitive ability of mice decreased significantly, and microglia secreted ADAM9 significantly. ADAM9 regulates pyroptosis of GHRH neurons by the Mad2L2-JNK-caspase-1 pathway. Sorafenib inhibits ADAM9 secretion by microglia and improves GH levels and the cognitive ability of mice. This study found that the crosstalk between GHRH neurons and neuroglial cells in the hypothalamic arcuate nucleus, i.e., microglia, is an essential factor in the formation of GHD in SAH. We propose that neutralization of ADAM9 production by microglia might be a potential therapy for GHD after SAH.

†Jian Mao, Yun Bao, Fan Liu and Qiyun Ye contributed equally to this work.

*Correspondence:
Songtao Qi
qisongtaonfyy@126.com
Jun Pan
1448875873@qq.com
Binghui Qiu
oceanmai1@126.com

Full list of author information is available at the end of the article

Graphical abstract

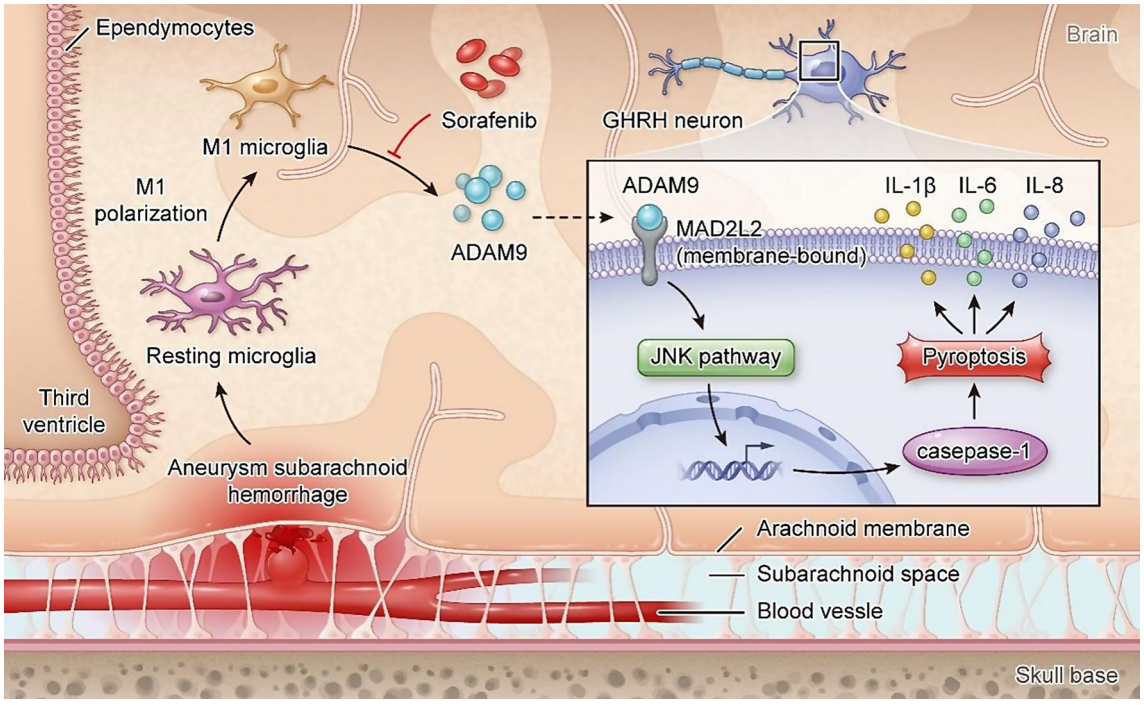

Keywords Subarachnoid hemorrhage, Pyroptosis, ADAM9, GHRH neuron, Microglia

Introduction

The annual incidence of subarachnoid hemorrhage (SAH) is 6–10/100,000 [1], and the fatality rate is as high as 50% [2]. Even after successful treatment, 67% of survivors are severely disabled [3]. Because the age of onset is generally young to middle-aged, it places heavy burdens on families and society. SAH typically occurs within the circle of Willis [4]. Since the circle of Willis is close to the hypothalamus, patients often have hypothalamic-related neuroendocrine dysfunction, and growth hormone deficiency (GHD) is the most common complication, even if disease progression is prevented [5]. Among the sequelae of SAH, the incidence of GHD is as high as 29% [6]. GHD causes energy synthesis disorders that result in cognitive degeneration, growth and development disorders, and increased mortality due to cardiovascular diseases. Therefore, GHD is an important risk factor for poor prognosis after SAH [7]. The specific causes of its pathogenesis need to be further studied.

Growth hormone releasing hormone (GHRH) neurons are located in the arcuate nucleus (ARC) of the hypothalamus, which is the highest center regulating GH secretion [8]. Once damaged, the entire growth hormone axis is directly affected. Microglia are one of three types of glial cells (the other two types are oligodendrocytes and tanycytes) in the ARC and are the main intracranial immune cells that can sense a slight imbalance of environmental homeostasis and activate quickly [9]. Activated microglia are divided into two polarized states: M1 (proinflammatory) and M2 (anti-inflammatory); microglia in different polarized states have different regulatory effects on neurons [10]. After the aneurysm ruptures, blood enters the subarachnoid space. Inflammation cascades, beginning with methemoglobin and heme produced by the breakdown of red blood cells. Microglia are mainly polarized to the M1 phenotype after inflammatory activation in SAH [11]. At this point, the cell body becomes larger, microglial process retraction becomes increasingly thicker and shorter, the expression of Toll-like receptor 4 (TLR4) and the nicotinamide adenine dinucleotide phosphate (NADPH) oxidase complex are upregulated, the transcription factor nuclear factor-κB (NF-κB) is activated, and a variety of neurotoxic factors are produced that affect neurons. Our previous studies have shown that the immune microenvironment in the saddle region regulates GH secretion through crosstalk between GH cells and stroma cells i.e. pericytes in GHD [12, 13]. Therefore, we hypothesized that after the occurrence of SAH, microglia in the ARC of the hypothalamus cause damage to GHRH neurons by secreting certain neurotoxic factors leading to GHD.

In this study, we analyzed the CSF of SAH patients by mass spectrometry and ELISA to screen for differentially expressed proteins associated with GHD. And we found that Disintegrin and metalloprotease 9 (ADAM9) was most associated with GHD after SAH. Next, we explored the cellular origin of ADAM9 and the potential molecular mechanisms regulating GHRH secretion by GHRH neurons in vivo. Finally, we tested drugs that inhibit ADAM9 secretion which can improved GHD after SAH.

Materials and methods

SAH patients

Forty cerebrospinal fluid (CSF) specimens and clinical data on age, sex, aneurysm location, aneurysmal size, Hunt & Hess score, Fisher grade, BMI, and GH were used in this study. Half of the specimens were used for mass spectrometry analysis, and the other half were used for the validation phase. Specimen and clinical data were collected from patients with acute nontraumatic SAH in the Department of Neurosurgery at Nanfang Hospital, Southern Medical University in Guangzhou, China, from September 2019 to August 2020. Patients who were admitted to the hospital within 24 h of ictus, presented with SAH, were diagnosed by initial brain computed tomography (CT) at onset, and were confirmed by digital subtraction angiography and/or computerized tomography angiography within 1–3 d of onset were included in the study. All patients were treated by endovascular coiling by a single cerebrovascular neurosurgeon. The study was carried out in accordance with The Code of Ethics of the World Medical Association (Declaration of Helsinki) and approved by the medical ethics committee of Nanfang Hospital, Southern Medical University, and patients consented to the use of their specimens for the study.

Diagnosis of GHD

GHD was detected two weeks after the operation. The body mass index (BMI) and peak GH values after the insulin stimulation test were recorded for all patients. The diagnosis of GHD was defined as a peak GH value of less than 3 ng/mL after effective stimulation based on an insulin stimulation test or less than 11 ng/mL if the BMI was below 25 kg/m^2, less than 8 ng/mL if the BMI was between 25 and 30 kg/m^2 and less than 4 ng/mL if the BMI was greater than 30 kg/m^2 according to an arginine+GHRH test [14].

Sample Preparation and Gel Electrophoresis

All CSF samples were obtained by lumbar puncture within 48 h of onset and placed in a 15 ml RNase/DNase-free centrifuge tube. The unfiltered CSF was centrifuged at 5000 × g at 4 °C for 10 min, and the supernatant was removed, transferred to 0.5 ml polypropylene tubes and stored at −80 °C until further analysis. CSF samples were coded and analyzed in a blinded fashion. SDT lysis buffer was added to the sample. The lysate was sonicated and then boiled for 15 min. After centrifugation at 14,000 × g for 40 min, the supernatant was quantified with a BCA Protein Assay Kit (P0012, Beyotime). The sample was stored at −20 °C. Twenty micrograms of protein from each sample was mixed with 6x loading buffer and boiled for 5 min. The proteins were separated on a 12.5% SDS–PAGE gel. Protein bands were visualized with Coomassie blue R-250 staining.

NanoLC–MS/MS (Nanoscale Liquid Chromatography coupled to Tandem Mass Spectrometry) analysis

The separated proteins were subjected to in-gel digestion before nanoLC–MS/MS analysis. The peptides were redissolved in solvent A (0.1% formic acid in water) and analyzed by online nanospray LC–MS/MS on an Orbitrap Exploris 480 coupled to an EASY-nLC 1200 system (Thermo Fisher Scientific, MA, USA). Two microliters of peptide sample was loaded on an analytical column (Thermo Fisher Scientific, Acclaim Pep Map RSLC 50 mm × 15 cm, nanoViper, P/N164943) and separated using a solvent B (0.1% formic acid, 80% ACN) gradient from 5 to 38% for 120 min. The column flow rate was maintained at 300 nl/min. An electrospray voltage of 2 kV relative to the inlet of the mass spectrometer was used. The mass spectrometer was run in data-independent acquisition mode and automatically switched between MS and MS/MS modes. The parameters were as follows: (1) MS: scan range (m/z)=350–1500; resolution=60,000; automated gain control (AGC) target=3e6; maximum injection time=50 ms; (2) higher-energy C-trap dissociation (HCD)–MS/MS: resolution=30,000; AGC target=1e6; collision energy=28; and (3) data-independent acquisition (DIA) performed with a variable isolation window, with each window overlapping 1 m/z, a window number of 42, and a total cycle time of 3 s.

Protein identification and quantification

The raw DIA data were processed and analyzed by Spectronaut X (Biognosys AG, Switzerland) with the default settings, and the retention time prediction type was set to dynamic indexed retention time (iRT). Data extraction was determined by Spectronaut X based on extensive mass calibration. Spectronaut Pulsar X dynamically determines the ideal extraction window depending on the iRT calibration and gradient stability. The Q value (false discovery rate, or FDR) cutoff at the precursor and protein levels was set to 1%. Decoy generation was set to be mutated, which is similar to "scrambled" but applied with a random number of AA position swaps (min=2, max=length/2). All selected precursors that passed through the filters were used for quantification. MS2 interference removes all interfering fragment ions

except for the three least interfering ions. The average of the top three filtered peptides that passed the 1% Q value cutoff were used to calculate the major group quantities. Protein abundance was quantified by the area under the chromatographic peak of the MS peptide precursor ion signal intensity. Student's *t* test was performed, and proteins were defined as differentially expressed if they had a p value < 0.05 and a fold change > 1.5.

Animals

A total of 565 male C57BL/6 mice (weight, 21 ± 2 g) were provided by the Laboratory Animal Center of Southern Medical University (Guangzhou, China). Mice had access to standard chow and water and were housed under standard laboratory conditions with a 12-h light–dark cycle at room temperature (RT) (24 ± 2 °C). All animal procedures were approved by the Animal Care Committee of Southern Medical University in accordance with the UK Animal Scientific Procedures Act 1986, the European Union (EU) Directive 2010/63/EU for animal experiments or the Guide for the Care and Use of Laboratory Animals published by the National Institutes of Health (NIH Publication No. 8023, revised in 1978). The study was approved by the Ethics Committee of Nanfang Hospital (ID: NFYY-2016-117). In addition, all efforts were made to minimize the number of animals used in the study and their suffering.

Mouse experiments

Endovascular perforation of the SAH was performed as we previously described [15]. Briefly, the mice were anesthetized, and a 5−0 nylon suture was advanced 3 mm past the bifurcation of the left internal carotid artery to induce arterial rupture, was withdrawn 3 mm and then readvanced 3 mm. In the sham group, the suture was not advanced past the internal carotid artery bifurcation. CSF was collected from the mice as previously described [16]. The sequences of primers used in the AAV were as follows: MAD2L2 (5′-CATCTTCCAGAAGCGCAAG AA-3′) and NC (5′-CAACAAGATGAAGAGCACCA A-3′).

Antibodies

The following primary antibodies were used: anti-ADAM9 (Thermo Fisher Scientific, Cat# PA5-76732, RRID: AB_2720459), anti-ADAM9 (Santa Cruz, Cat# sc-135822, RRID: AB_2221762), anti-Iba1 (Wako, Cat# 011-27991, RRID: AB_2935833), anti-CD11b (Abcam, Cat# ab184308, RRID: AB_2889154), GHRH (Thermo Fisher Scientific, Cat# PA5-92408, RRID: AB_2806480), GSDMD (Proteintech, Cat# 66387-1-Ig, RRID: AB_2881763), MAD2L2 (BD Biosciences Cat# 612266, RRID: AB_399583)), GFAP (Novus Cat# NBP2-33184DL594, RRID: AB_2923514), Olig2 (Proteintech, Cat# 66513-1-Ig, RRID: AB_2881876), NeuN (Abcam, Cat# ab104224, RRID: AB_10711040), caspase-1 (Abcam, Cat# ab207802, RRID: AB_2889889), GAPDH (Abcam, Cat# ab8245, RRID: AB_2107448), P-JNK (CST, Cat# 9255 S, RRID: AB_2307321), JNK (CST, Cat# 9252 S, RRID: AB_2250373), P-ERK (CST, Cat# 4370 S, RRID: AB_2315112), ERK (CST, Cat# 4695 S, RRID: AB_390779), P-p38 (CST, Cat# 9216 S, RRID: AB_331296), and p38 (CST, Cat# 8690 S, RRID: AB_10999090).

Tissue preparation for histology and immunostaining

Mice were euthanized using an i.p. injection of sodium pentobarbitone (1.6 mg/g BW), before being transcardially perfused with phosphate buffered saline (PBS) and 4% formalin. Brains were dissected, placed in formalin for 24 h, followed by PBS with 0.01% sodium azide. Tissue was cryoprotected in 30% sucrose with 0.05% sodium azide for 2 days. Free-floating serial brain Sect. (40 mm) were collected using a sliding microtome (Leica).

Immunofluorescence

For immunofluorescence staining of coronal frozen brain sections, the sections were rinsed with PBS, followed by blocking with 5% nonspecific-antigen goat serum for 1 h at 37 °C. Then, the sections were incubated overnight at 4 °C with specific primary antibodies. The next day, after rinsing with PBS containing 0.5% Triton X-100 three times, the sections were incubated for 1 h at 37 °C with the corresponding secondary antibodies conjugated to Alexa 488 or Alexa 594 (Thermo Fisher Scientific, USA). The primary and secondary antibodies were diluted in PBS containing 5% normal goat serum and 0.2% Triton X-100. After incubation with secondary antibodies, the sections were mounted on glass slides, and cover slips were applied in mounting medium. Fluorescence images were captured with a confocal microscope (LSM880, Zeiss, Germany). For cell counts, the data are presented as the number of cells/mm^2. For double-staining analysis, the data are presented as the ratio of the number of double-positive cells to the number of single-positive cells.

Morris water maze

The Morris water maze (MWM) test was performed as previously described [17]. Briefly, the first 5 d are dedicated to acquisition training. On day 6, the number of platform crossings and the time spent in the target quadrant were determined.

Open field test

The open-field arena test was performed using a Versamax animal activity monitor equipped with infrared photobeams as horizontal X–Y sensors and/or Z sensors. Mice were placed in the center of the open-field

arena (40 cm × 40 cm × 30 cm) and allowed to explore for 60 min. The locomotor activity and location of the mice were scored automatically by VersaMax software. The percentage of time spent in the center area indicates anxiety levels.

Nissl staining

After the mice were perfused with 0.1 mol/L PBS followed by 4% paraformaldehyde (PFA), brain slices were removed, immersed in 4% PFA for 24 h and transferred to 30% sucrose solution until they sank. Subsequently, the brain slices were cut into 20 μm-thick transverse and horizontal sections using a freezing microtome (Thermo, USA). After the sections were incubated with 0.1% cresyl violet for 5 min at RT, the sections were rinsed in double distilled water followed by 95% ethanol, dehydrated in 100% ethanol, cleared in xylene, and covered in neutral resins. Images were acquired with a microscope (Nikon, Tokyo, Japan), and the neurons were counted with ImageJ software (Media Cybernetics, Bethesda, MD, USA).

Western blot

Western blot analyses were performed with an SDS–PAGE system. Briefly, total extracted tissue was lysed with RIPA buffer containing protease inhibitor and protein phosphatase inhibitors at 4 °C for 30 min. The protein concentration was determined using a BCA assay kit (Beyotime Inc., China). Protein samples were separated using SDS-PAGE and transferred to polyvinylidene difluoride (PVDF) membranes (Millipore, USA). Then, the membranes were blocked with 5% BSA and incubated with primary antibodies overnight at 4 °C. The next day, after washing with TBST, the membranes were incubated with secondary antibodies for 1 h at RT. Finally, signals were detected using enhanced chemiluminescence reagents, and images were captured with a digital camera (Pierce, Rockford, IL, USA). The total gray value of each band was quantified with ImageJ software (NIH) and normalized to that of the loading control.

ELISA

ELISA was performed in accordance with the manufacturer's protocol. The following kits and antibodies were used: a human ADAM9 ELISA kit (EHADAM9×10; Thermo Fisher; USA), an NPTX1 polyclonal antibody (20656-1-AP; Proteintech; USA), a YWHAB polyclonal antibody (10936-1-AP; Proteintech; USA), a mouse GH ELISA kit (EZRMGH-45 K; Millipore; USA), a mouse ACTH ELISA kit (ab263880; abcam; USA), a mouse PRL ELISA kit (ab214572; abcam; USA), a mouse TSH ELISA kit (EEL110; Thermo Fisher; USA), a mouse interleukin (IL)-1β ELISA kit (BMS6002TEN; Thermo Fisher; USA), a mouse IL-6 ELISA kit (E-EL-M0044; Elabscience; China), and a mouse IL-8 ELISA kit (abs520017; Absin; China).

Isolation and treatment of GHRH neurons and microglia

Mice were decapitated after inhalation anesthesia with isoflurane to obtain the whole brain. The hypothalamic ARC was dissected into single cells using successive incubations in 0.25% trypsin-EDTA. GHRH neurons were suspended, and microglia were adherent. The medium was replaced when the cells crawled out. For GHRH neurons, the medium was replaced with serum-free medium (DMEM/F12 containing 0.5% bovine serum albumin (BSA), B27, and N2 supplements in addition to 20 ng/mL bFGF and EGF). For microglia, freshly dissected cells were cultured in Dulbecco's modified Eagle medium (DMEM) supplemented with 10% fetal bovine serum (FBS). The cells were incubated at 37 °C and 5% CO_2.

Single-cell RNA-seq analysis

Single-cell RNA-seq data and t-SNE projections were downloaded from https://tabula-muris.ds.czbiohub.org/; specifically, single-cell libraries from 100,605 cells were isolated from 20 organs from 3 female and 4 male 3-month-old C57BL/6JN mice. Gene count files were derived from cells prepared using the 10x Genomics platform and processed with CellRanger.

Statistical analysis

The results are expressed as the mean ± SD from at least three independent experiments and were analyzed by using GraphPad Prism 9 or SPSS 22.0 software (IBM, Armonk, NY, USA). Continuous variables with a normal distribution were compared using independent Student's *t* tests, and those without a normal distribution were evaluated by nonparametric tests (Western blot, ELISA, and immunocytochemistry). In the MWM test, we averaged the escape latencies across the four trials for each mouse. These means were analyzed across five sessions. Two-way repeated-measures ANOVA was used for the main effect, with session as the repeated measure and escape latency as the dependent variable. A two-tailed probability value of <0.05 was considered to indicate statistical significance. * represents $p<0.05$; ** represents $p<0.01$; *** represents $p<0.001$.

Results

A high level of ADAM9 in CSF is associated with GHD after SAH

Based on clinical data (Table 1), SAH patients were divided into GHD and NO-GHD groups, and CSF from the two groups was analyzed by mass spectrometry. A total of 75 proteins were differentially regulated in the CSF between the two groups; specifically, 39 proteins were upregulated, and 36 proteins were downregulated, with thresholds of $p<0.05$ and |fold change| >1.5. The expression of proteins in each sample of the two groups is shown in a heatmap (Fig. S1A). The significance level

Table 1 Baseline characteristics of the patients with subarachnoid hemorrhage

Variables	Development cohort (*n* = 20)		*P* value	Validation cohort (*n* = 20)		*P* value
	GHD (*n* = 10)	No-GHD (*n* = 10)		GHD (*n* = 10)	No-GHD (*n* = 10)	
Age, y	52.6 ± 12.195	49.6 ± 6.132	0.496	46.1 ± 10.775	50.7 ± 8.629	0.306
Gender						
Male, %	1(10)	1(10)		3 (30)	2 (20)	
Female, %	9(90)	9(90)		7 (70)	8 (80)	
Aneurysm Location						
AcoA, %	6(60)	3(30)		5 (50)	4 (40)	
PcoA, %	2(20)	3(30)		3 (30)	3 (30)	
MCA, %	2(20)	4(40)		2 (20)	3 (30)	
Aneurysmal size (mm)	6.22 ± 3.247	3.845 ± 0.959	**0.049**	5.828 ± 1.516	3.197 ± 0.639	**<0.001**
Hunt & Hess score	3 (2–4)	2 (1–3)	0.063	3 (2–4)	2 (1–4)	**0.009**
Fisher grade	4 (2–4)	3 (1–4)	**0.019**	4 (3–4)	2 (1–4)	**0.001**
BMI	24 ± 2.867	24.2 ± 2.53	0.87	24.3 ± 2.452	24.2 ± 3.765	0.945
Peak GH (ng/mL)	3.5 (2.094–6.74)	11.2 (8.59–13.15)	**<0.001**	5.28 ± 2.077	12.223 ± 1.784	**<0.001**

and magnitude of changes in the quantitative data are visualized in a volcano plot (Fig. 1A). The results of principal component analysis showed that the GHD group and NO-GHD group could be distinguished significantly at the protein expression level. This result indicated that GHD in SAH patients may be closely related to protein expression in CSF (Fig. S1B). To elucidate the potential biological functions of all differentially expressed proteins, the target genes of these proteins were predicted, and functional enrichment analysis was performed. According to the GO analysis results, 2,264 biological process (BP), 351 cellular component (CC), and 410 molecular function (MF) terms were significantly enriched. The significantly enriched biological processes are shown in Fig. S1C, including the apoptotic signaling pathway in response to DNA damage, the negative regulation of axonogenesis, the MAPK cascade, protein folding in the endoplasmic reticulum, NF-κB signaling, the neuronal apoptotic process, and the cellular response to oxidative stress. The top 20 enriched pathways according to the KEGG enrichment analysis are shown in Fig. 1B. The enrichment pathway results showed that the MAPK signaling pathway, which is involved in neuronal death, was significantly enriched. The datasets presented in this study can be found in online repositories. The names of the repository/repositories and accession number(s) can be found below: http://proteomecentral.proteomexchange.org/cgi/GetDataset? ID=PXD032118.

We selected 4 proteins (ADAM9, YWHAB, NPTX-1 and CLU) for further verification by ELISA. We selected these specific proteins from the differentially expressed proteins in the proteomics analysis based on a literature analysis focusing on the following points: the magnitude (fold change) and significance of the expression difference in CSF, protein expression enrichment in the brain, protein function, antibody availability, and/or a previous description of a possible association with neuronal damage. The expression of the 4 candidate proteins from the screening phase was further analyzed in the CSF of a cohort of SAH patients using ELISA (Fig. 1C-F). Receiver operating characteristic curve analysis was carried out to evaluate the predictive value of these 4 candidate proteins for GHD. We then performed ROC analysis on these proteins. As shown in Fig. 1G, the ROC curve demonstrated that the AUC was 0.98 for ADAM9, 0.91 for YWHAB, 0.9 for NPYX-1 and 0.84 for CLU, with a cutoff value, 95% confidence interval (CI), and sensitivity and specificity values, as shown in table S1. We found that the ADAM9 gene was expressed in multiple brain regions, including the hypothalamus (Fig. S2A-B), through a public database (https://www.proteinatlas.org/). ADAM9 is a secretory membrane-anchored protein that participates in development, birth, immune function, signal transduction, neurodegenerative disease and cancer, primarily through the disintegrin domain for adhesion and through the metalloprotease domain for ectodomain shedding of a wide variety of cell surface proteins [18]. We also found that the ADAM9 gene was expressed in a variety of intracranial cells, including microglia (Fig. S2C-D), through a single-cell sequencing database provided by The Tabula Muris Consortium [19]. Therefore, the above results suggest that a high level of ADAM9 in CSF is associated with GHD after SAH.

The damage of GHRH neurons is the main cause of GHD after SAH

For further exploration in vivo, we first induced the classical SAH mouse model (Fig. 2A). We determined the changes in the mice on different days. Here we used NeuN as a marker of mature neurons and GHRH as a marker of GHRH neurons. The anatomical location of the arcuate

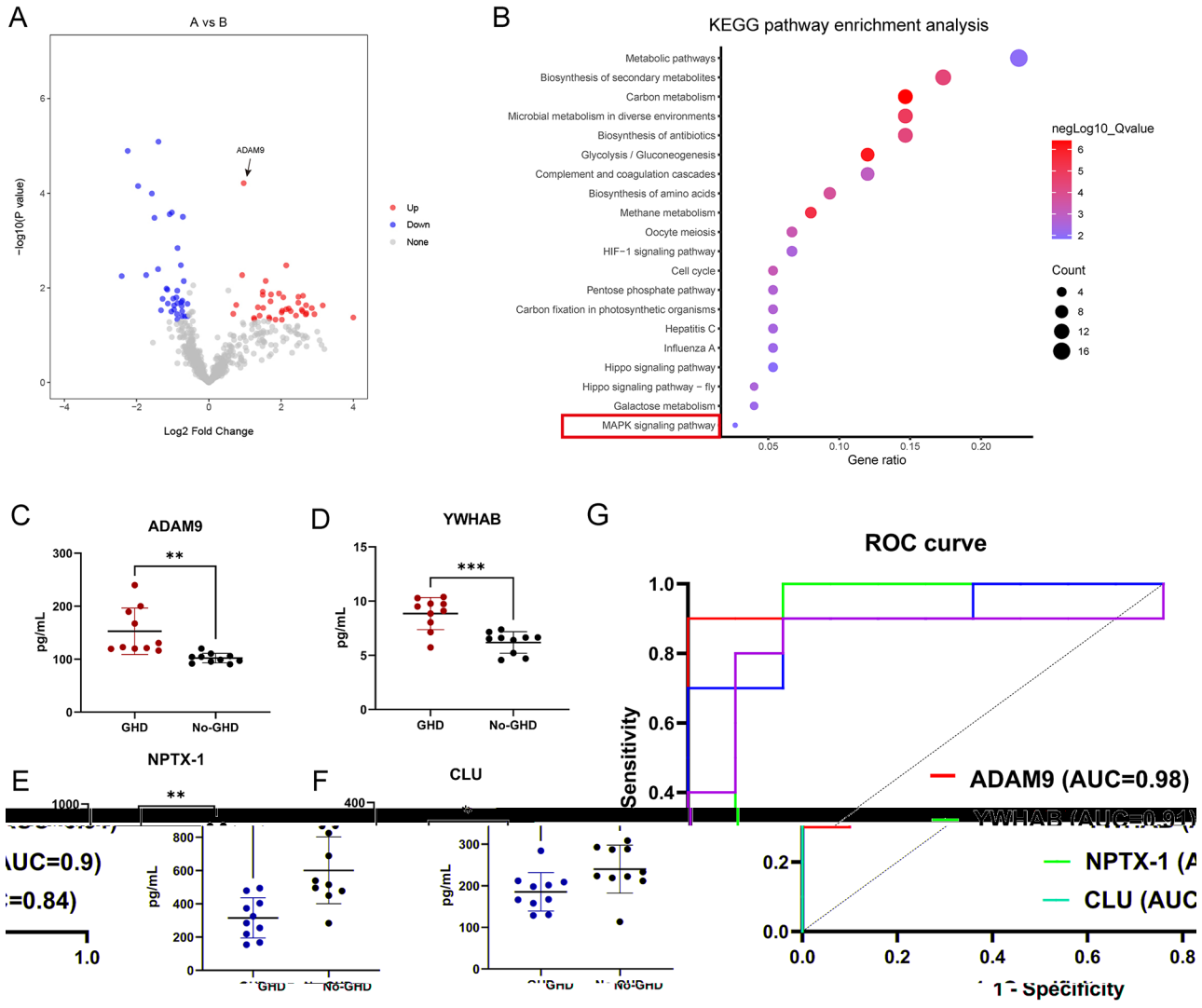

Fig. 1 Exploring the key protein in CSF that associated with GHD after SAH. (**A**) Volcano plot showing differentially expressed proteins between the two groups. The horizontal axis indicates $\log_2$ (fold change). The vertical axis indicates − 10 log *p* values. Each dot represents a protein, and dots in red and blue have a fold change > 1.5 and *p* value < 0.05, as determined by Student's *t* test. The gray dots represent proteins with no statistically significant differences in expression. The arrow points to ADAM9. (**B**) KEGG analysis of intersecting genes. The bubble pattern shows the top 20 enrichment pathways according to enrichment score, gene count, and *p* value. (**C**-**F**) CSF levels of the candidate proteins in the GHD group ($n = 10$) compared to those in the No-GHD group ($n = 10$), which was consistent with the mass spectrometry data. (**G**) The area under the curve (AUC) values of the candidate proteins determined by receiver operating characteristic (ROC) curve analysis suggest that ADAM9 has the strongest correlation with GHD

nucleus was shown in Fig. 2B. The results of immunofluorescence and Nissl's staining showed that the number of GHRH neurons (Fig. 2C-D, S3A-B) decreased significantly on day 7. And the GH and cognitive abilities of the mice similarly declined most at day 7. (Fig. 2E-I). The results of the open field test suggested that the decrease in Morris water maze performance in the 7 d and 14 d groups was not caused by decreased motor ability of the mice (Fig. S3C). To further rule out the effect of SAH on the pituitary gland in vivo, histological sections of pituitary gland were stained with hematoxylin and eosin staining (H&E staining). Fig. S3D reveal that no noticeable damage or inflammatory lesions were observed, suggestive of no effect on the pituitary gland. Similar results were observed when other endocrine hormones were assessed (Fig. S3E-G). According to the above experiments, we found that the damage of GHRH neuron0s in the hypothalamus is a major cause of GHD and cognitive decline after SAH, and the GHRH neurons of the mice decreased most significantly on the 7th day after SAH.

ADAM9 released by microglia induces pyroptosis in GHRH neurons in SAH

First, we verified that ADAM9 was differentially (highly) expressed in the CSF of SAH mice (Fig. 3A). The expression of ADAM9 increased significantly on day 7

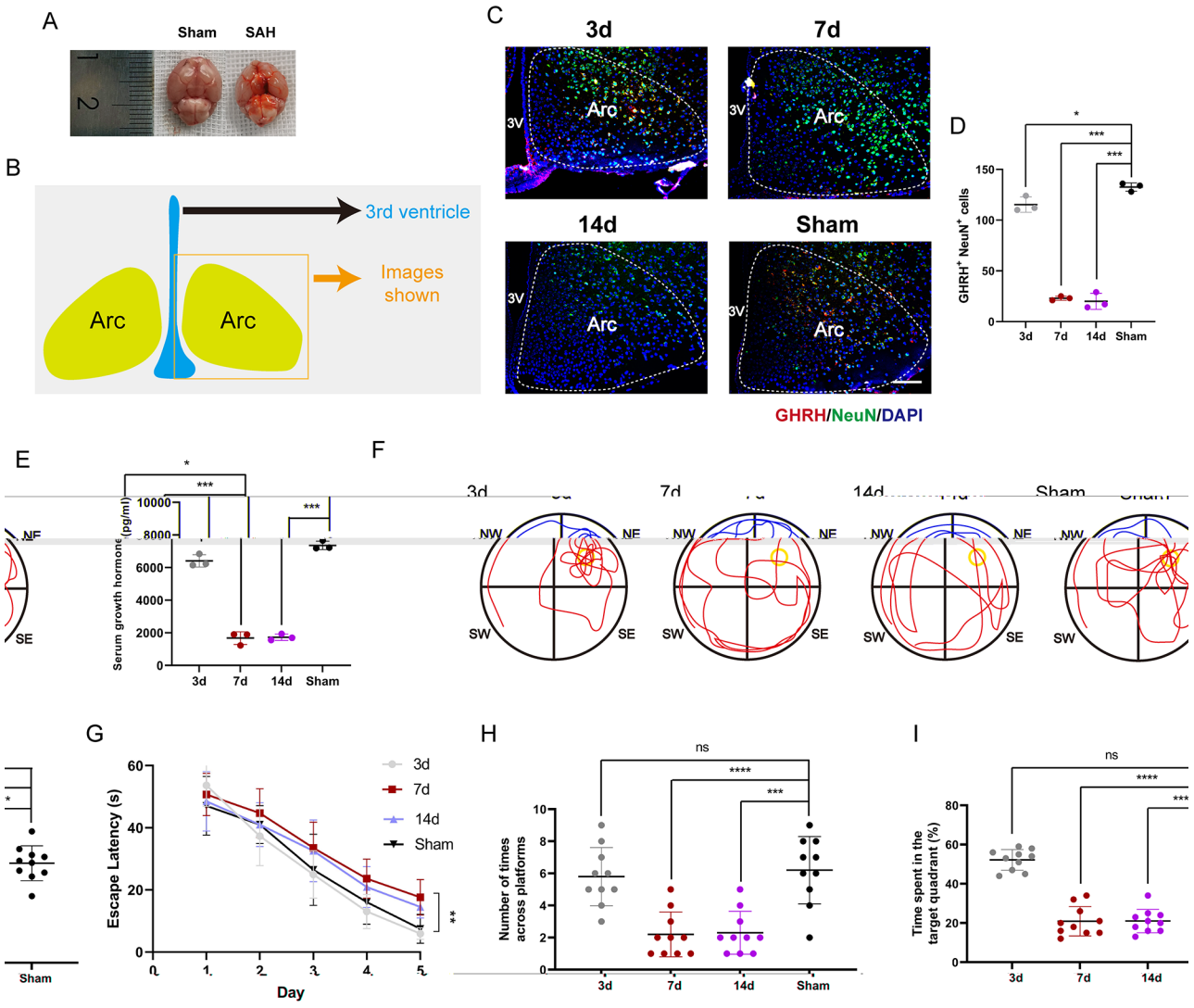

Fig. 2 Exploring the temporal changes of GHD after SAH in vivo. (**A**) Photos of the SAH surgery. (**B**) Schematic diagram of the anatomical location of the arcuate nucleus. (**C**) The number of GHRH neurons at 3 d, 7 d and 14 d after SAH surgery was measured by immunofluorescence and compared to sham-operated mice. Scale bar = 100 μm. (**D**) Quantification of C. $n = 3$. (**E**) The expression of GH at 3 d, 7 d and 14 d after SAH surgery was measured by ELISA. $n = 3$. (**F**-**I**) The cognitive ability of mice at 3 d, 7 d and 14 d after SAH surgery was measured by the Morris water maze. $n = 10$. ARC: Arcuate nucleus. 3 V: The third ventricle. * $p < 0.05$; ** $p < 0.01$; *** $p < 0.001$

(Fig. 3B-C). However, we found that the ADAM9 protein was not expressed in GHRH neurons (Fig. 3D). In addition to neurons, the cells in the hypothalamic arcuate nucleus are mainly glial cells, including microglia, oligodendrocytes and tanycytes [20]. Microglia can be activated into two states, M1 and M2. M2 microglia are branched, and M1 microglia are amoebic [21]. We used Iba-1 as a marker of mciroglia, GFAP as a marker of tanycytes, Olig2 as a marker of oligodendrocytes. Through immunofluorescence colocalization experiments, we found that ADAM9 was mainly expressed in microglia, a small amount was expressed in tanycytes (Fig. 3B-C, S4). We therefore determined the status of microglia in the SAH 7 d group. We used Iba-1 as a marker for microglia and CD11b as a marker for M1 microglia. Immunofluorescence colocalization experiments indicated that microglia in the hypothalamus tissue of the SAH 7 d group exhibited M1 morphology (Fig. 3E) and expressed ADAM9 (Fig. 3F). Pyroptosis is a type of caspase-1-mediated programmed necrosis that cleaves GSDMD to form N-terminal free peptides and induces cell rupture to release inflammatory factors [22]. Western blot analysis of hypothalamic ARC tissues revealed that caspase-1 expression was significantly higher in the SAH 7 d group than in the sham group (Fig. 3G-H). The expression of GSDMD was significantly increased in GHRH neurons in the SAH 7 d group (Fig. 3I-J). The levels of the inflammatory factors IL-1β, IL-6 and IL-8 were significantly

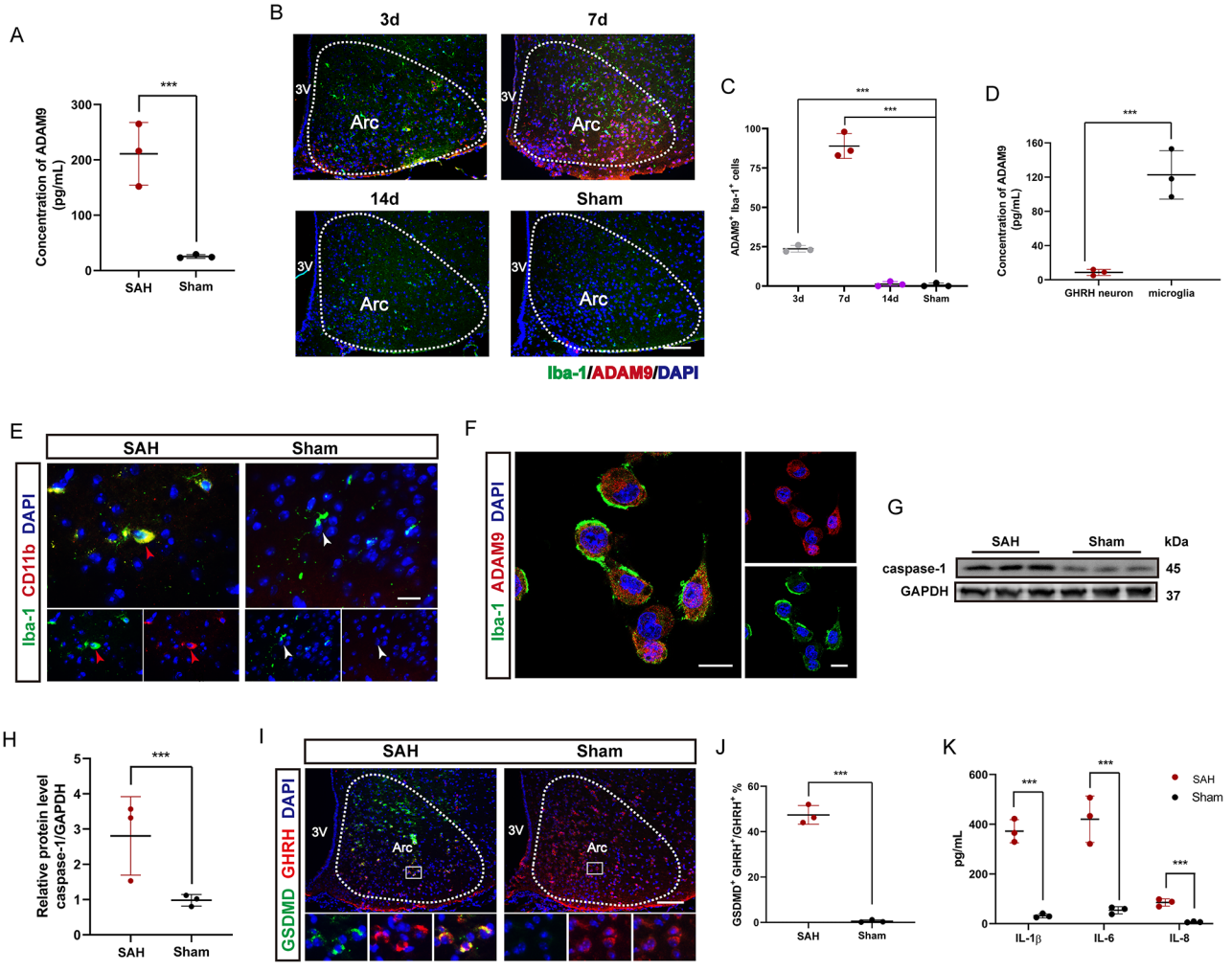

Fig. 3 ADAM9 induces pyroptosis in GHRH neurons in SAH. (**A**) The content of ADAM9 in the CSF of mice on day 7 after SAH surgery was significantly greater than that in the CSF of sham-operated mice. $n = 3$. (**B**) The expression of ADAM9 and the activation of microglia at 3 d, 7 d and 14 d after SAH surgery compared with those in sham-operated mice. Iba-1 is a microglial marker. Scale bar = 100 μm. (**C**) Quantification of B. $n = 3$. (**D**)The content of ADAM9 in the supernatant of GHRH neurons. Microglial supernatant was used as a positive control. $n = 3$. (**E**) CD11b and Iba-1 were coexpressed in the SAH group, and microglia were more strongly activated in the SAH group than in the sham-operated group. CD11b is an M1 microglial marker. The arrow indicates microglia. Scale bar = 20 μm. (**F**) ADAM9 and Iba-1 were coexpressed in hypothalamic microglia in primary culture on day 7 after SAH surgery. Scale bar = 20 μm. (**G**) Caspase-1 was highly expressed in the ARC at 7 days after SAH surgery. GAPDH expression was used to confirm equal protein loading and blotting. (**H**) Quantification of G. $n = 3$. (**I**) Immunofluorescence showed that the number of $GHRH^+$ $GSDMD^+$ neurons in the SAH group was significantly greater than that in the control group. (**J**) Quantification of the ARC in I. $n = 3$. (**K**) The expression of IL-1β, IL-6 and IL-8 in the ARC on day 7 after SAH surgery was significantly higher than that in the sham-operated mice. $n = 3$. ARC: Arcuate nucleus. 3 V: The third ventricle. * $p < 0.05$; *** $p < 0.001$

increased in the ARC of the hypothalamus in the SAH 7 d group (Fig. 3K). These results was to test if ADAM9 is released by M1 microglia leads to GHRH neuron pyroptosis in SAH.

Changes in hypothalamic microglia affect GH and cognitive ability in SAH mice

Since we previously confirmed that ADAM9 released by microglia has an important effect on GHD, we next speculated whether changes in the state of microglia itself can affect GHD. With this in mind, we constructed two mouse models. In the first model, mice were fed PLX3397 (600 mg/kg) [23] or control chow for 14 d to eliminate microglia, while the SAH model was induced on day 7 (Fig. 4A). The number of microglia in the ARC in the PLX3397 group was significantly decreased, and the expression of ADAM9 was also decreased (Fig. 4B-C). We found that the expression of GSDMD in GHRH neurons was significantly decreased in the PLX3397 group (Fig. 4D-E). The level of caspase-1 in the ARC was decreased in the PLX3397 group (Fig. 4F-G). The expression of IL-1β, IL-6 and IL-8 decreased in the ARC of the PLX3397 group (Fig. 4H). GH levels and cognitive ability were increased in mice in the PLX3397 group (Fig. 4I-M). These results preliminarily suggest that microglial removal can improve GHD after SAH.

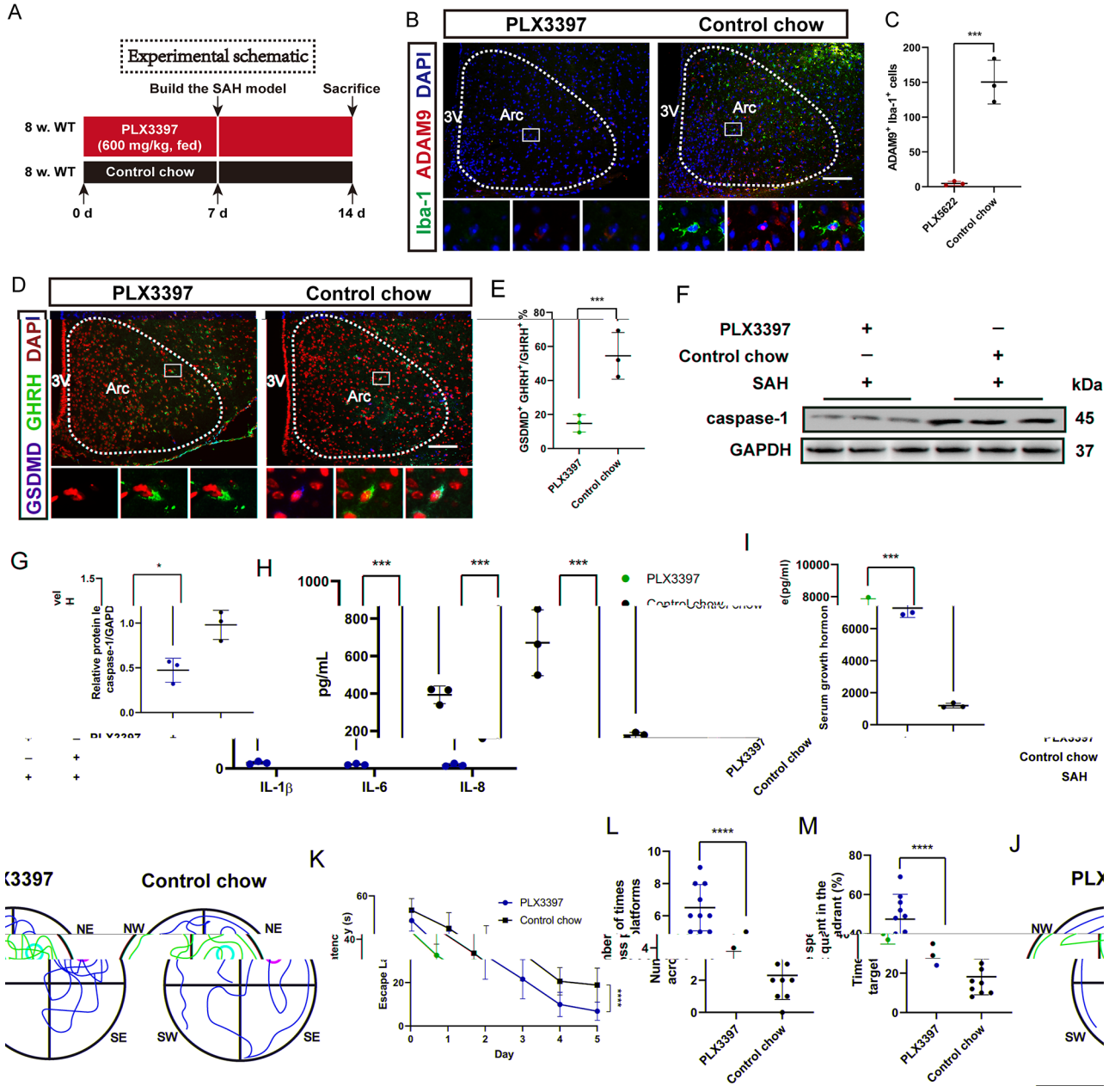

Fig. 4 GH and cognitive changes in SAH mice after elimination of hypothalamic microglia. (**A**) Schematic representation of SAH surgery involving the elimination of microglia. (**B**) After the use of PLX3397, the number of microglia and the expression of ADAM9 decreased at 7 days after SAH surgery compared with those in control chow-fed mice. Scale bar = 100 μm. (**C**) Quantification of the data in B. $n = 3$. (**D**) After the use of PLX3397, the expression of GSDMD in GHRH neurons decreased on day 7 after SAH surgery. Scale bar = 100 μm. (**E**) Quantification of the ARC in D. $n = 3$. (**F**) After the use of PLX3397, the expression of caspase-1 in the ARC decreased at 7 days after SAH surgery. GAPDH expression was used to confirm equal protein loading and blotting. (**G**) Quantification of F. $n = 3$. (**H**) After treatment with PLX3397, the expression levels of 1β, IL-6 and IL-8 were decreased in the ARC at 7 days after SAH surgery. $n = 3$. (**I**) The expression of GH increased in the PLX3397 group. $n = 3$. (**J**-**M**) Cognitive ability improved in the PLX3397 group. $n = 10$. ARC: Arcuate nucleus. 3 V: The third ventricle. * $p < 0.05$; ** $p < 0.01$; *** $p < 0.001$

To detect cognition and development after M1 microglial polarization, we then induced a mouse model of microglial activation by i.p. injection of LPS (0.33 mg/kg) [24] or PBS for 3 days. Microglia in the ARC were significantly activated, and ADAM9 was highly expressed (Fig. S5A-B). We found that GSDMD expression was significantly increased in GHRH neurons in the LPS group (Fig. S5C-D). The level of caspase-1 in the ARC was increased in the LPS group (Fig. S5E-F). The expression levels of IL-1β, IL-6 and IL-8 were increased in the ARC of the LPS group (Fig. S5G). GH levels and cognitive ability were decreased in mice in the LPS group (Fig. S5H-L).

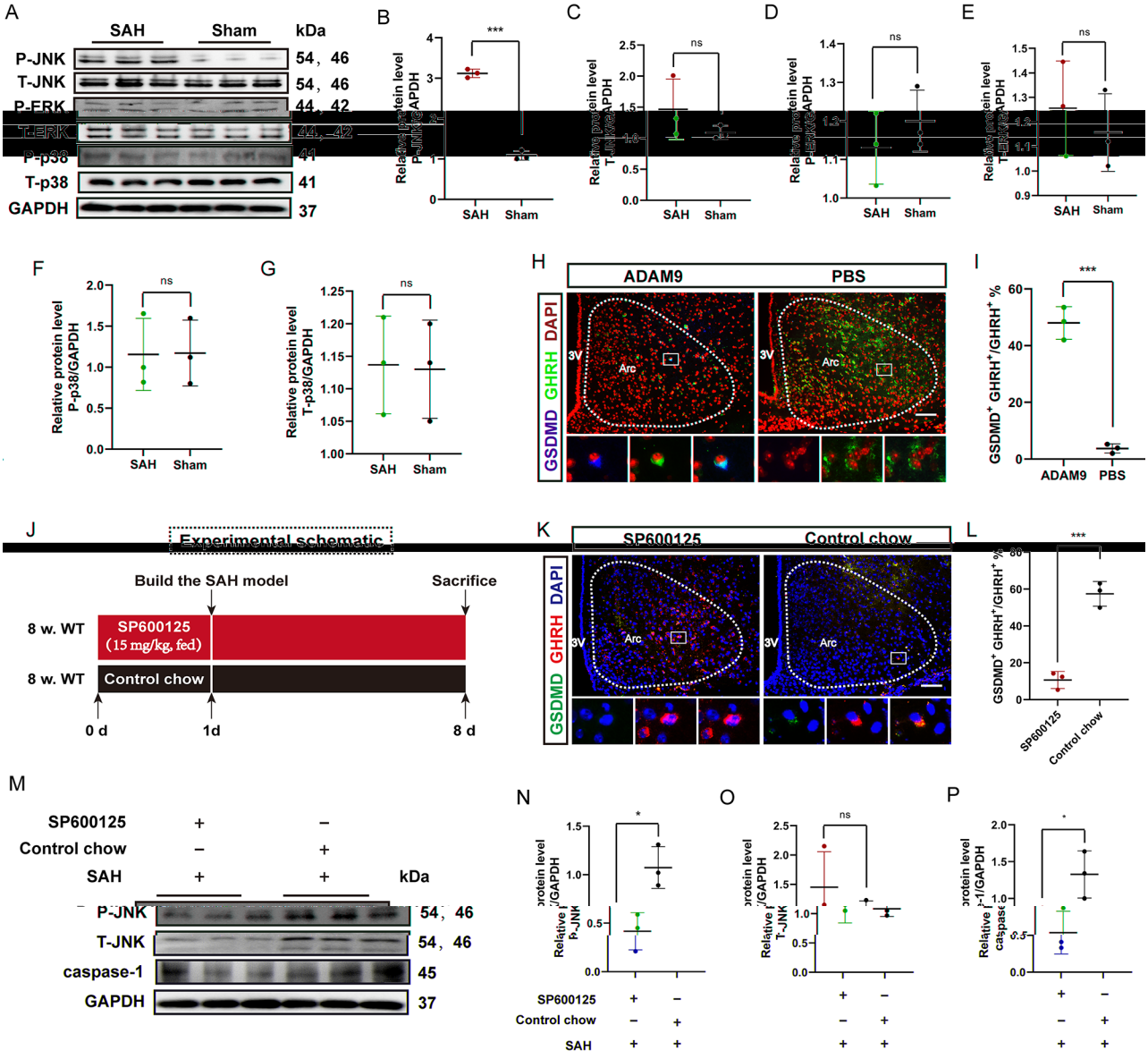

Fig. 5 ADAM9 induces pyroptosis in GHRH neurons via the JNK pathway. (**A**) Protein levels of JNK, ERK and p38 pathway markers were measured on day 7 postsurgery in SAH and sham-operated mice by Western blot. GAPDH was used as a loading control. (**B-G**) Quantification of A. $n = 3$. (**H**) The expression of GSDMD in GHRH neurons was increased when ADAM9 was injected into the ARC. Scale bar = 100 μm. (**I**) Quantification of the ARC in H. $n = 3$. (**J**) Schematic representation of SAH surgery after blocking the JNK pathway. (**K**) After SP600125 treatment, the expression of GSDMD in GHRH neurons decreased at 7 days after SAH surgery. Scale bar = 100 μm. (**L**) Quantification of the ARC in K. $n = 3$. (**M**) After the use of SP600125, the protein levels of JNK and pyroptosis pathway markers were measured on day 7 postsurgery in SAH and sham-operated mice by Western blotting. GAPDH was used as a loading control. (**N-P**) Quantification of M. $n = 3$. ARC: Arcuate nucleus. 3 V: The third ventricle. * $p < 0.05$; *** $p < 0.001$

These results suggest that the activation of microglia can induce GHRH neuron pyroptosis and GHD.

ADAM9 induces pyroptosis in GHRH neurons through the JNK pathway

Based on the results of enrichment analysis, the MAPK pathway was significantly enriched (Fig. 1B), and ADAM9 is involved in the regulation of the MAPK pathway. The MAPK pathway is divided into three branches: the JNK, ERK and p38 pathways [25]. We next attempted to determine which of these three pathways is involved in ADAM9-induced GHRH neuron pyroptosis. We performed Western blot analysis of these three pathways in the hypothalamic ARC, and the results indicated that only the JNK pathway was activated in the SAH group (Fig. 5A-G).

We injected the mouse ARC with recombinant ADAM9 protein (1 μL/h) [26] or PBS for 7 days via the stereo-oriented microcapsule sustained release technique. The specific steps were the same as previously

described [12]. The coordinates are 0.4 mm, 1.46 mm, and 5.6 mm. We demonstrated that GHRH neurons undergo pyroptosis (Fig. 5H-I). To confirm that ADAM9 causes pyroptosis in GHRH neurons via the JNK pathway, SP600125 (15 mg/kg) or control chow for 1 d was used to inhibit the JNK pathway, and then an SAH model was induced (Fig. 5J). Western blot results confirmed that the JNK pathway was inhibited (Fig. 5M-O). We found that GSDMD decreased in GHRH neurons in the SAH group when the JNK pathway was inhibited (Fig. 5K-L), and caspase-1 also decreased in the ARC in the SAH group (Fig. 5M, P). These results indicate that ADAM9 leads to Caspase-1-dependent GHRH neuron pyroptosis via the JNK pathway.

Blocking MAD2L2 inhibits ADAM9-induced activation of the JNK pathway and pyroptosis in GHRH neurons

We next wanted to explore how microglia-derived ADAM9 activates the JNK pathway in GHRH neurons. We found through the STRING database (https://cn.string-db.org) that MAD2L2 is a protein that interacts with ADAM9. MAD2L2 is an adaptor protein whose interaction network with various proteins has yet to be elucidated. MAD2L2 is a key player in coordinating the cellular response to DNA damage [27]. First, MAD2L2 was shown to be involved in the G1 phase of DNA synthesis in neurons in the above single-cell sequencing database (Fig. S2E-F). We then detected increased MAD2L2 expression in GHRH neurons in both SAH mice and ARC-injected ADAM9 mice (Fig. 6A-D). We therefore used AAV to knock out MAD2L2 (Fig. 6E-F, J-K) and then induced an SAH model. 500 nL of pAAV-U6-shRNA(MAD2L2)-CMV-EGFP-WPRE or pAAV-U6-shRNA(NC)-CMV-EGFP-WPRE was injected into the ARC of the mice (titer: 1.0E+12), and the mice were observed for one month. We found that the JNK-caspase-1 pathway was decreased in SAH mice when MAD2L2 was knocked out (Fig. 6E, G-I). Moreover, GSDMD was also decreased in GHRH neurons (Fig. 6L-M). GH levels and cognitive ability were increased in mice in the KO MAD2L2+SAH group (Fig. 6N-R). These results suggest that ADAM9 activates the JNK-caspase-1 pathway through MAD2L2, leading to pyroptosis in GHRH neurons.

Sorafenib improves GHD after SAH by inhibiting ADAM9 expression in microglia

Since ADAM9 secreted by microglia strongly influences GHD after SAH, we sought to determine whether blocking ADAM9 secreted by microglia would improve GHD. Here, sorafenib was used as an inhibitor of ADAM9 secretion by microglia [18]. Mice were fed sorafenib (30 mg/kg) [28] or control chow for 7 days during the induction of the SAH model. Immunofluorescence results indicated that ADAM9 was inhibited after sorafenib administration, while microglia were not affected (Fig. 7A-B). We found that MAD2L2 decreased in GHRH neurons in sorafenib-treated SAH mice (Fig. 7C-D). GSDMD expression decreased in GHRH neurons (Fig. 7E-F). The JNK-caspase-1 pathway was downregulated in the ARC tissues (Fig. 7G-J). The expression of IL-1β, IL-6 and IL-8 decreased in the ARC tissues (Fig. 7K). GH and cognitive ability improved (Fig. 7L-P). These results suggest that sorafenib blocks GHRH neuron pyroptosis by inhibiting the expression of ADAM9 in microglia, thus improving GHD after SAH.

Discussion

This study analyzed and verified CSF from SAH patients by mass spectrometry and ELISA. ROC curve analysis was performed on the expression of various proteins and GHD, and it was found that ADAM9 had the strongest correlation with GHD. In the SAH mouse model, we found that ADAM9 originates from M1-type microglia in the hypothalamus and regulates the pyroptosis of GHRH neurons by activating the MAD2L2-JNK-caspase-1 axis, ultimately leading to GHD. Sorafenib inhibits ADAM9 secretion by microglia and improves GH levels and cognitive ability in mice.

Clinical evidence of GHD after SAH is growing [29]. The occurrence GHD after SAH is believed to be related to the proximity of the circle of Willis to the hypothalamic-pituitary complex [6, 30]. Previous studies have mostly examined gross anatomy as the cause. As early as 1951, A. Ecker and P. A. Riemenschneider et al.. reported stenosis of large arteries near the circle of Willis in 6 of 29 patients with SAH [31]. Since then, cerebral vasospasm characterized by vascular stenosis has been considered the main cause of delayed brain injury in patients with SAH. However, drugs for preventing vasospasm have not achieved positive clinical effects. Subsequent studies suggested that the compression of aneurysms on the hypothalamic-pituitary complex was the main cause of endocrine dysfunction [32]. But we found that no noticeable damage or inflammatory lesions were observed in the pituitary gland, suggestive of no effect on the pituitary gland after SAH. Similar results were observed when endocrine hormones (ACTH/PRL/TSH) were assessed. Evidence also suggests that endocrine dysfunction, especially GHD, can still occur after surgery to remove the compression of the aneurysm on the hypothalamic-pituitary complex [29]. In addition, recent evidence suggests that neuroinflammation plays a key role in brain injury after SAH. Red blood cell breakdown products can lead to the release of inflammatory factors, which can trigger vasospasm and tissue damage [33]. However, our mass spectrometry results suggested that there was no significant difference in inflammatory factors. It is suggested

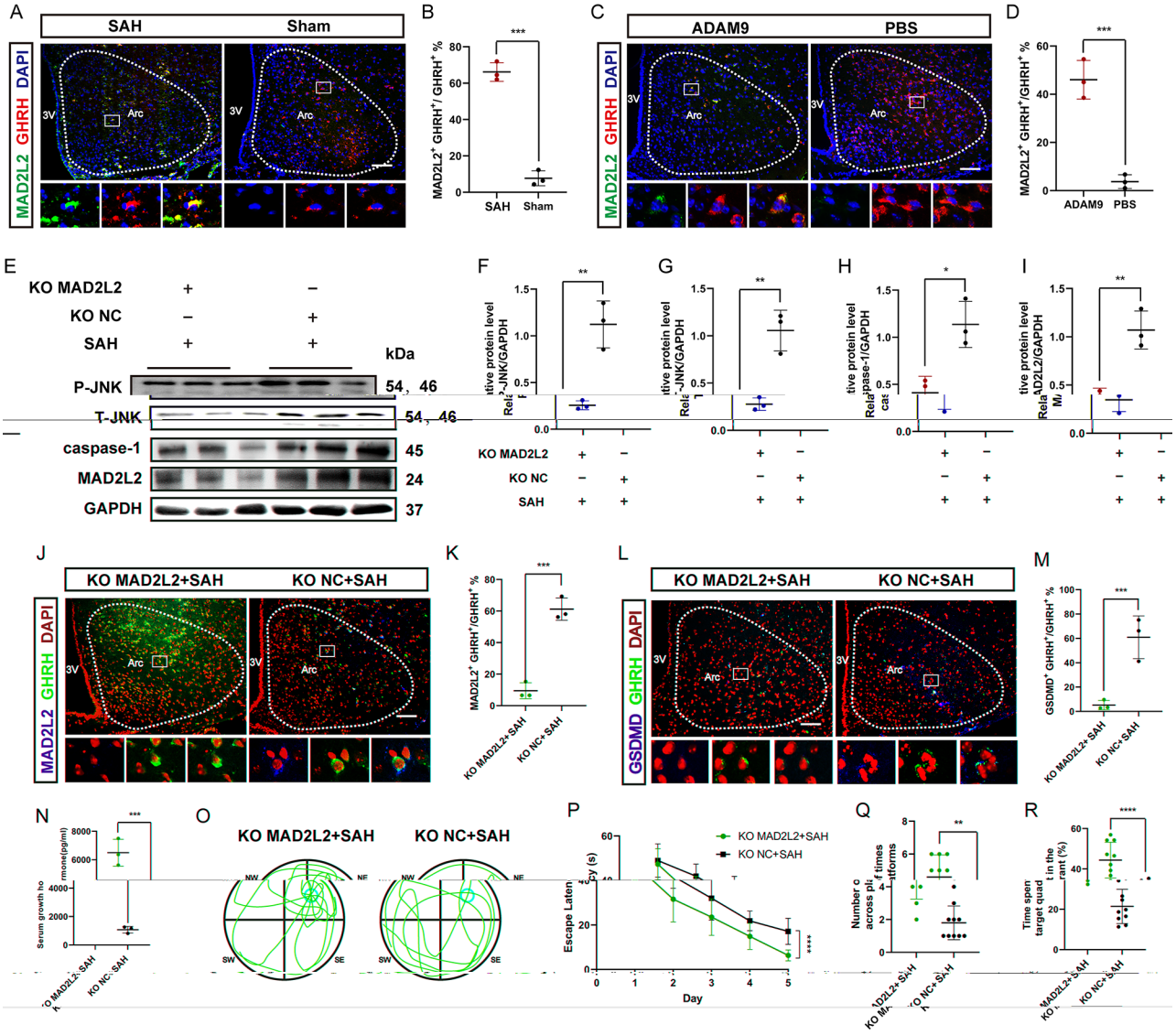

Fig. 6 Changes in GHRH neurons after MAD2L2 KO in SAH mice. (**A**) The expression of MAD2L2 in GHRH neurons was higher on day 7 postsurgery in SAH mice than in sham-operated mice. Scale bar = 100 μm. (**B**) Quantification of the ARC in A. $n = 3$. (**C**) The expression of MAD2L2 in GHRH neurons was higher when ADAM9 was injected into the ARC than when it was injected into the PBS. Scale bar = 100 μm. (**D**) Quantification of the ARC in C. $n = 3$. (**E**) After MAD2L2 KO, the protein levels of the JNK pathway markers caspase-1 and MAD2L2 were measured on day 7 postsurgery in SAH mice by Western blotting. GAPDH was used as a loading control. (**F**-**I**) Quantification of E. $n = 3$. (**J**) After MAD2L2 KO, the expression of MAD2L2 in GHRH neurons was decreased on day 7 postsurgery in SAH mice. Scale bar = 100 μm. (**K**) Quantification of the ARC in J. $n = 3$. (**L**) After MAD2L2 KO, the expression of GSDMD in GHRH neurons was decreased on day 7 postsurgery in SAH mice. Scale bar = 100 μm. (**M**) Quantification of the ARC in L. $n = 3$. (**N**)The expression of GH increased in the KO MAD2L2 + SAH group. $n = 3$. (**O**-**R**) Cognitive ability improved in the KO MAD2L2 + SAH group. $n = 10$. ARC: Arcuate nucleus. 3 V: The third ventricle. * $p < 0.05$; ** $p < 0.01$; *** $p < 0.001$

that other pathophysiological mechanisms besides cerebral vasospasm and neuroinflammation may play a role in GHD after SAH. This study focused on the molecular mechanism, considering that the Willis circle is close to the hypothalamic ARC, and the highest number of central GHRH neurons secreting GH are in the hypothalamic ARC. Due to ethical limitations, we can only initiate our study from a patient's CSF. We conducted mass spectrometry analysis and subsequent validation of patient-derived CSF, and found that ADAM9 is a key factor in GHD after SAH.

ADAM9, an ADAM protein, was first identified in 1996 in breast carcinoma [34]. It is widely expressed in human tissues and is greatly increased under pathological conditions [35]. ADAM9 expression has been detected in a variety of cell types, including monocytes [36], macrophages [37], neutrophils [38], and fibroblasts [39], and in a variety of organs, including the nervous system [40] and endocrine system [41]. ADAM9 has also been shown to

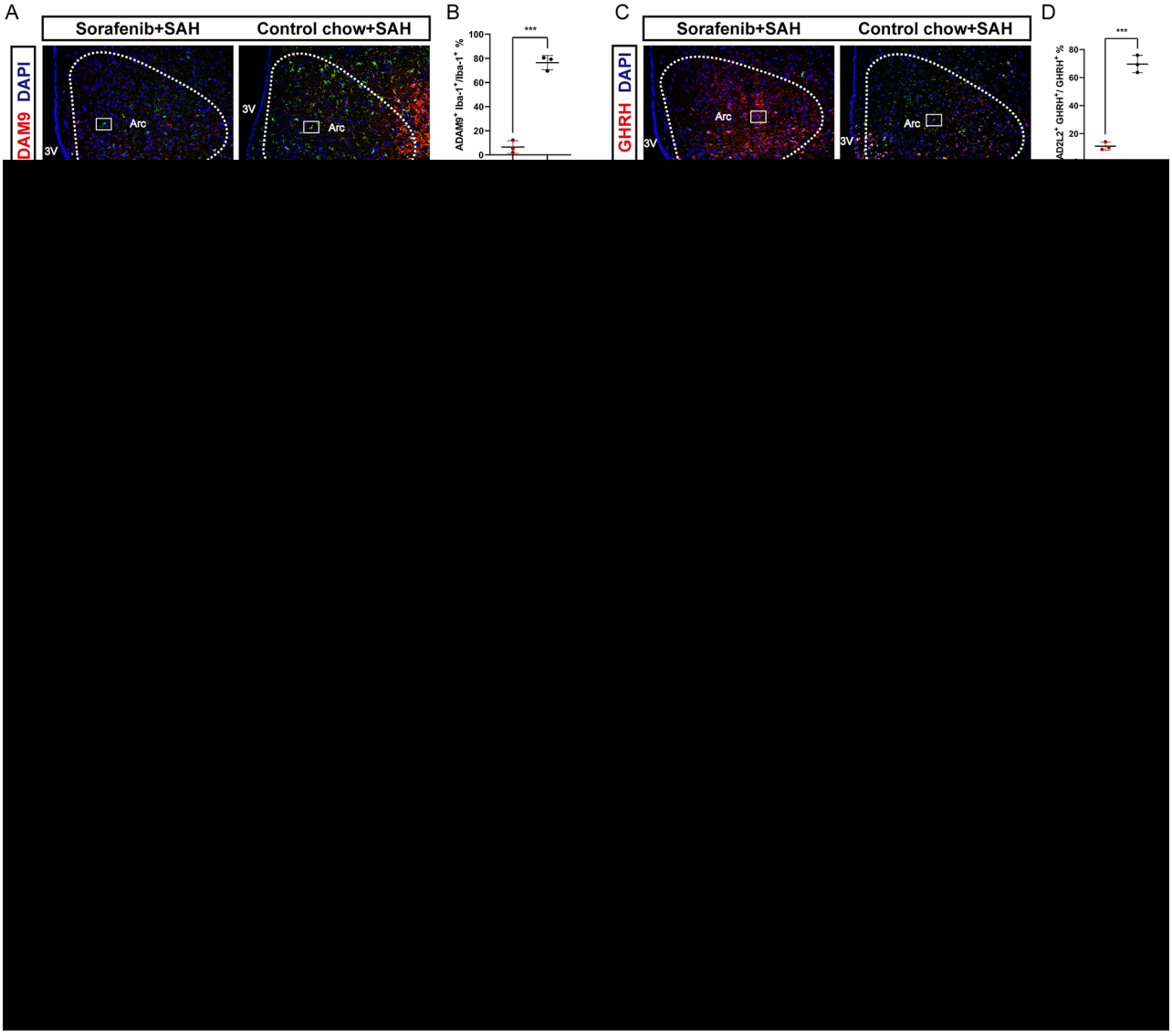

Fig. 7 The effect of sorafenib on SAH mice. (**A**) There was no significant change in the number of microglia in SAH mice after the administration of sorafenib. However, the expression of ADAM9 decreased. Scale bar = 100 μm. (**B**) Quantification of the ARC in A. $n = 3$. (**C**) The expression of MAD2L2 in GHRH neurons was decreased in SAH mice after treatment with sorafenib. Scale bar = 100 μm. (**D**) Quantification of the ARC in C. $n = 3$. (**E**) The expression of GSDMD in GHRH neurons was decreased in SAH mice after the administration of sorafenib. Scale bar = 100 μm. (**F**) Quantification of the ARC in E. $n = 3$. (**G**) After treatment with sorafenib, the protein levels of JNK pathway markers and caspase-1 were measured in SAH mice by Western blotting. GAPDH was used as a loading control. (**H-J**) Quantification of G. $n = 3$. (**K**) After treatment with sorafenib, the expression levels of 1β, IL-6 and IL-8 were decreased in the ARC of SAH mice. $n = 3$. (**L**) After the use of sorafenib, the expression of GH increased in SAH mice. $n = 3$. (**M-P**) After the use of sorafenib, the cognitive ability of SAH mice improved. $n = 10$. ARC: Arcuate nucleus. 3 V: The third ventricle. * $p < 0.05$; ** $p < 0.01$; *** $p < 0.001$

be involved in neurodegenerative diseases by regulating the cleavage of amyloid precursor protein (APP), which may be associated with Alzheimer's disease [42]. This finding suggested that ADAM9 is involved in multiple biological functions and pathophysiological mechanisms, such as inflammation and tumorigenesis. In this study, we first ruled out ADAM9 expression in GHRH neurons. In addition to neurons, the most common cell types in the brain are glial cells, including tanycytes, oligodendrocytes and microglia. We used markers corresponding to the three types of cells in combination with ADAM9 and found that ADAM9 was derived from hypothalamic microglia.

Neuronal death is not only a "cell-autonomous" event. It is usually triggered by interactions with neighboring neurons and glial cells. Currently, there are at least a dozen known modes of neuronal death, including apoptosis, iron-dependent death, pyroptosis and autophagy [43]. Caspase-1-mediated programmed necrosis-mediated pyroptosis was first identified in bacterium-infected

macrophages [22]. Procaspase-1 is first cleaved into active caspase-1 during pyroptosis. Then, gasdermin-d (GSDMD) is cleaved to release its N-terminal domain, which binds membrane lipids and punches holes in the cell membrane, resulting in cell rupture due to changes in osmotic pressure and the release of IL-1β, IL-6 and IL-8. Microglial regulation of pyroptosis in various neurons in the brain has been confirmed in cerebral ischemia–reperfusion [44], Parkinson's disease [45], spinal cord injury [46] and other diseases but has not been reported in SAH. SAH can induce a variety of stress events, including a rapid increase in intracranial pressure, a marked decrease in cerebral perfusion pressure, brain edema, and a decrease in heme load caused by erythrocyte lysis. The aggregation of these stress events often leads to the immune response of microglia [47]. In vivo, we found that caspase-1 and GSDMD were increased in GHRH neurons in the SAH 7 d group, as was the expression of IL-1β, IL-6 and IL-8. However, when microglia were cleared in advance, caspase-1 and GSDMD were decreased in GHRH neurons, and IL-1β, IL-6 and IL-8 were also decreased. These results indicate that after SAH, microglia are involved in the pyroptosis of GHRH neurons.

The results of the enrichment analysis showed that the MAPK pathway was significantly enriched and that ADAM9 was involved in the regulation of the MAPK pathway. Therefore, we hypothesized that ADAM9 may regulate pyroptosis in GHRH neurons through the MAPK pathway. Three members of the MAPK family have been characterized: classic MAPK (also known as extracellular signal-regulated kinase (ERK)), C-Jun N-terminal kinase/stress-activated protein kinase (JNK/SAPK) and p38 kinase [25]. The JNK pathway is generally the "death" signaling pathway. It controls the cell's response to harmful extracellular stimuli such as inflammatory cytokines and ultraviolet radiation from gamma rays. These harmful stimuli translocate JNKs into the nucleus, where they bind to and activate transcription factors, leading to DNA mutations or damage. If DNA damage cannot be repaired immediately, cells must be programmed to die to avoid these undesirable mutations or damage [48]. Our results suggest that only the JNK pathway is upregulated and that the pyroptosis of GHRH neurons is significantly blocked after the use of JNK pathway inhibitors. These results suggest that the JNK pathway is involved in ADAM9-induced pyroptosis in GHRH neurons. ADAM9 is a membrane-anchored protein, so we speculate that ADAM9 activates downstream signaling pathways by binding to membrane proteins on GHRH neurons. Through screening and verification, we confirmed the intermediate protein MAD2L2.

Microglia have both beneficial and deleterious effects that maintain the advantage of activating a complete cytokine cascade that kills harmful foreign pathogens and polarizes T cells to produce an adaptive immune response and the disadvantage of being activated by inflammation and releasing neurotoxic factors that damage or kill neurons [49]. Therefore, the elimination of microglia is not an effective option for the treatment of related diseases. Following our literature review, we found that ADAM9 is a key target involved in the occurrence and development of diseases such as lung injury [38], myocarditis, encephalitis [50] and a variety of tumors [51–53]. In this study, we found that sorafenib could improve the pyroptosis of GHRH neurons and GHD after SAH by targeting ADAM9 secretion by microglia.

In conclusion, in this study, we found that microglia in the ARC undergo M1-type polarization and secrete ADAM9 after SAH, which activates the JNK signaling pathway in GHRH neurons through the adaptor protein MAD2L2, thereby initiating the caspase-1-dependent pyroptosis program, which ultimately leads to GHD. Sorafenib blocks the pyroptosis of GHRH neurons and GHD by inhibiting the release of ADAM9 by microglia. These findings provide a promising therapeutic target for overcoming GHD after SAH.

Supplementary Information

The online version contains supplementary material available at https://doi.org/10.1186/s12974-024-03299-x.

Supplementary Material 1

Supplementary Material 2

Author contributions

Jian Mao, Yun Bao, and Fan Liu performed primary data analysis and wrote the manuscript. Jian Mao, Qiyun Ye, Junxiang Peng, Jing Nie, and Wenfeng Feng performed the experiments related to preclinical animal studies. Jian Mao, Lijun Huang, and Yonghong Liao performed the immunofluorescence and ELISA. Jian Mao, Yiheng Xing, Dongyang Wu, and Ke Wang performed the Western blotting and histological staining. Songtao Qi, Jun Pan, and Binghui Qiu designed and supervised the study. All authors edited and approved the final manuscript.

Funding

This study was supported by the Chinese National Natural Science Foundation (82200870), President Foundation of Nanfang Hospital, Southern Medical University (2021C011), and Funding by Science and Technology Projects in Guangzhou (2023A04J2334).

Data availability

No datasets were generated or analysed during the current study.

Declarations

Competing interests

The authors declare no competing interests.

Author details

[1]Department of Neurosurgery, Institute of Brain Diseases, Nanfang Hospital, Southern Medical University, Guangzhou 510515, China
[2]Guangdong Sanjiu Brain Hospital, Guangzhou 510515, China
[3]Department of Neurosurgery, The First Affiliated Hospital of Jinan University, Guangzhou 510515, China

[4]The First Clinical College, Southern Medical University, Guangzhou 510515, China

Received: 23 July 2024 / Accepted: 13 November 2024
Published online: 19 November 2024

References

1. Schneider HJ, Kreitschmann-Andermahr I, Ghigo E, Stalla GK, Agha A. Hypothalamopituitary dysfunction following traumatic brain injury and subarachnoid hemorrhage: a systematic review. JAMA. 2007;298(12):1429–38.
2. Al-Khindi T, Macdonald RL, Schweizer TA. Cognitive and functional outcome after subarachnoid hemorrhage. Stroke. 2010;41(8):e519–36.
3. Petridis AK, Kamp MA, Cornelius JF, Beez T, Beseoglu K, Turowski B, et al. Subarachnoid hemorrhage. Dtsch Arztebl Int. 2017;114(13):226–36.
4. Kreitschmann-Andermahr I. Subarachnoid hemorrhage as a cause of hypopituitarism. Pituitary. 2005;8(3–4):219–25.
5. Kelly DF, Gonzalo IT, Cohan P, Berman N, Swerdloff R, Wang C. Hypopituitarism following traumatic brain injury and subarachnoid hemorrhage: a preliminary report. J Neurosurg. 2000;93(5):743–52.
6. Khajeh L, Blijdorp K, Neggers SJ, Ribbers GM, Dippel DW, van Kooten F. Hypopituitarism after subarachnoid haemorrhage, do we know enough? BMC Neurol. 2014;14:205.
7. Profka E, Rodari G, Giacchetti F, Giavoli CGH. Deficiency and replacement therapy in Hypopituitarism: insight into the relationships with other hypothalamic-pituitary axes. Front Endocrinol (Lausanne). 2021;12:678778.
8. Zhou F, Zhang H, Cong Z, Zhao LH, Zhou Q, Mao C, et al. Structural basis for activation of the growth hormone-releasing hormone receptor. Nat Commun. 2020;11(1):5205.
9. Prinz M, Jung S, Priller J. Microglia Biology: one century of evolving concepts. Cell. 2019;179(2):292–311.
10. Kwon HS, Koh SH. Neuroinflammation in neurodegenerative disorders: the roles of microglia and astrocytes. Transl Neurodegener. 2020;9(1):42.
11. Qu W, Cheng Y, Peng W, Wu Y, Rui T, Luo C, et al. Targeting iNOS alleviates early brain Injury after experimental subarachnoid hemorrhage via promoting ferroptosis of M1 Microglia and reducing Neuroinflammation. Mol Neurobiol. 2022;59(5):3124–39.
12. Mao J, Qiu B, Mei F, Liu F, Feng Z, Fan J, et al. Interleukin-1alpha leads to growth hormone deficiency in adamantinomatous craniopharyngioma by targeting pericytes: implication in pituitary fibrosis. Metabolism. 2019;101:153998.
13. Mao J, Huang H, Liu F, Mai Y, Liao X, Qiu B, et al. Activation of Age-Related Nuclear factor-kappab signaling pathway leads to chronic inflammation and Pituitary Fibrosis. World Neurosurg. 2022;157:e417–23.
14. Ho KK, Participants GHDCW. Consensus guidelines for the diagnosis and treatment of adults with GH deficiency II: a statement of the GH Research Society in association with the European Society for Pediatric Endocrinology, Lawson Wilkins Society, European Society of Endocrinology, Japan Endocrine Society, and Endocrine Society of Australia. Eur J Endocrinol. 2007;157(6):695–700.
15. Tao M, Mao J, Bao Y, Liu F, Mai Y, Guan S, et al. A blood-responsive AIE Bioprobe for the Ultrasensitive Detection and Assessment of Subarachnoid Hemorrhage. Adv Sci (Weinh). 2023;10(8):e2205435.
16. Liu L, Duff K. A technique for serial collection of cerebrospinal fluid from the cisterna magna in mouse. *J Vis Exp.* 2008(21).
17. Vorhees CV, Williams MT. Morris water maze: procedures for assessing spatial and related forms of learning and memory. Nat Protoc. 2006;1(2):848–58.
18. Chou CW, Huang YK, Kuo TT, Liu JP, Sher YP. An overview of ADAM9: structure, activation, and Regulation in Human diseases. Int J Mol Sci 2020;21(20).
19. Tabula Muris C et al. Overall c, Logistical c, Organ c, processing, Library p,. Single-cell transcriptomics of 20 mouse organs creates a Tabula Muris. *Nature.* 2018;562(7727):367 – 72.
20. Morrens J, Van Den Broeck W, Kempermann G. Glial cells in adult neurogenesis. Glia. 2012;60(2):159–74.
21. Lee E, Eo JC, Lee C, Yu JW. Distinct features of Brain-Resident macrophages: Microglia and Non-parenchymal Brain macrophages. Mol Cells. 2021;44(5):281–91.
22. Brennan MA, Cookson BT. Salmonella induces macrophage death by caspase-1-dependent necrosis. Mol Microbiol. 2000;38(1):31–40.
23. Spangenberg EE, Lee RJ, Najafi AR, Rice RA, Elmore MR, Blurton-Jones M, et al. Eliminating microglia in Alzheimer's mice prevents neuronal loss without modulating amyloid-beta pathology. Brain. 2016;139(Pt 4):1265–81.
24. Hoogland IC, Houbolt C, van Westerloo DJ, van Gool WA, van de Beek D. Systemic inflammation and microglial activation: systematic review of animal experiments. J Neuroinflammation. 2015;12:114.
25. Fang JY, Richardson BC. The MAPK signalling pathways and colorectal cancer. Lancet Oncol. 2005;6(5):322–7.
26. Feng Y, Li Q, Chen J, Yi P, Xu X, Fan Y, et al. Salivary protease spectrum biomarkers of oral cancer. Int J Oral Sci. 2019;11(1):7.
27. Li Y, Li L, Chen M, Yu X, Gu Z, Qiu H, et al. MAD2L2 inhibits colorectal cancer growth by promoting NCOA3 ubiquitination and degradation. Mol Oncol. 2018;12(3):391–405.
28. Ricci MS, Kim SH, Ogi K, Plastaras JP, Ling J, Wang W, et al. Reduction of TRAIL-induced Mcl-1 and cIAP2 by c-Myc or sorafenib sensitizes resistant human cancer cells to TRAIL-induced death. Cancer Cell. 2007;12(1):66–80.
29. Can A, Gross BA, Smith TR, Dammers R, Dirven CM, Woodmansee WW, et al. Pituitary Dysfunction after subarachnoid hemorrhage: a systematic review and Meta-analysis. Neurosurgery. 2016;79(2):253–64.
30. Ioachimescu AG, Barrow DL. Subarachnoid hemorrhage and the Pituitary. World Neurosurg. 2015;83(6):1026–8.
31. Ecker A, Riemenschneider PA. Arteriographic demonstration of spasm of the intracranial arteries, with special reference to saccular arterial aneurysms. J Neurosurg. 1951;8(6):660–7.
32. Crompton MR. Hypothalamic lesions following the rupture of cerebral berry aneurysms. Brain. 1963;86:301–14.
33. Lucke-Wold BP, Logsdon AF, Manoranjan B, Turner RC, McConnell E, Vates GE, et al. Subarachnoid hemorrhage and neuroinflammation: a Comprehensive Review. Int J Mol Sci. 2016;17(4):497.
34. Weskamp G, Kratzschmar J, Reid MS, Blobel CP. MDC9, a widely expressed cellular disintegrin containing cytoplasmic SH3 ligand domains. J Cell Biol. 1996;132(4):717–26.
35. Rinchai D, Kewcharoenwong C, Kessler B, Lertmemongkolchai G, Chaussabel D. Increased abundance of ADAM9 transcripts in the blood is associated with tissue damage. F1000Res. 2015;4:89.
36. Namba K, Nishio M, Mori K, Miyamoto N, Tsurudome M, Ito M, et al. Involvement of ADAM9 in multinucleated giant cell formation of blood monocytes. Cell Immunol. 2001;213(2):104–13.
37. Wang X, Polverino F, Rojas-Quintero J, Zhang D, Sanchez J, Yambayev I et al. A disintegrin and a Metalloproteinase-9 (ADAM9): a novel proteinase culprit with Multifarious contributions to COPD. Am J Respir Crit Care Med. 2018.
38. Roychaudhuri R, Hergrueter AH, Polverino F, Laucho-Contreras ME, Gupta K, Borregaard N, et al. ADAM9 is a novel product of polymorphonuclear neutrophils: regulation of expression and contributions to extracellular matrix protein degradation during acute lung injury. J Immunol. 2014;193(5):2469–82.
39. Abety AN, Fox JW, Schonefuss A, Zamek J, Landsberg J, Krieg T, et al. Stromal fibroblast-specific expression of ADAM-9 modulates proliferation and apoptosis in melanoma cells in vitro and in vivo. J Invest Dermatol. 2012;132(10):2451–8.
40. Hsia HE, Tushaus J, Brummer T, Zheng Y, Scilabra SD, Lichtenthaler SF. Functions of 'A disintegrin and metalloproteases (ADAMs)' in the mammalian nervous system. Cell Mol Life Sci. 2019;76(16):3055–81.
41. Grutzmann R, Luttges J, Sipos B, Ammerpohl O, Dobrowolski F, Alldinger I, et al. ADAM9 expression in pancreatic cancer is associated with tumour type and is a prognostic factor in ductal adenocarcinoma. Br J Cancer. 2004;90(5):1053–8.
42. Zhang P, Shen M, Fernandez-Patron C, Kassiri Z. ADAMs family and relatives in cardiovascular physiology and pathology. J Mol Cell Cardiol. 2016;93:186–99.
43. Fricker M, Tolkovsky AM, Borutaite V, Coleman M, Brown GC. Neuronal cell death. Physiol Rev. 2018;98(2):813–80.
44. Liu X, Zhang M, Liu H, Zhu R, He H, Zhou Y, et al. Bone marrow mesenchymal stem cell-derived exosomes attenuate cerebral ischemia-reperfusion injury-induced neuroinflammation and pyroptosis by modulating microglia M1/M2 phenotypes. Exp Neurol. 2021;341:113700.
45. Gordon R, Albornoz EA, Christie DC, Langley MR, Kumar V, Mantovani S et al. Inflammasome inhibition prevents alpha-synuclein pathology and dopaminergic neurodegeneration in mice. Sci Transl Med 2018;10(465).
46. Li X, Yu Z, Zong W, Chen P, Li J, Wang M, et al. Deficiency of the microglial Hv1 proton channel attenuates neuronal pyroptosis and inhibits inflammatory reaction after spinal cord injury. J Neuroinflammation. 2020;17(1):263.

47. van Lieshout JH, Dibue-Adjei M, Cornelius JF, Slotty PJ, Schneider T, Restin T, et al. An introduction to the pathophysiology of subarachnoid hemorrhage. Neurosurg Rev. 2018;41(4):917–30.
48. Nishina H, Wada T, Katada T. Physiological roles of SAPK/JNK signaling pathway. J Biochem. 2004;136(2):123–6.
49. Wan S, Cheng Y, Jin H, Guo D, Hua Y, Keep RF, et al. Microglia activation and polarization after Intracerebral Hemorrhage in mice: the role of protease-activated Receptor-1. Transl Stroke Res. 2016;7(6):478–87.
50. Baggen J, Thibaut HJ, Hurdiss DL, Wahedi M, Marceau CD, van Vliet ALW et al. Identification of the cell-surface protease ADAM9 as an entry factor for Encephalomyocarditis Virus. mBio 2019;10(4).
51. Lin CY, Chen HJ, Huang CC, Lai LC, Lu TP, Tseng GC, et al. ADAM9 promotes lung cancer metastases to brain by a plasminogen activator-based pathway. Cancer Res. 2014;74(18):5229–43.
52. Hua Y, Liang C, Miao C, Wang S, Su S, Shao P, et al. MicroRNA-126 inhibits proliferation and metastasis in prostate cancer via regulation of ADAM9. Oncol Lett. 2018;15(6):9051–60.
53. Oh S, Park Y, Lee HJ, Lee J, Lee SH, Baek YS et al. A disintegrin and metalloproteinase 9 (ADAM9) in Advanced Hepatocellular Carcinoma and their role as a Biomarker during Hepatocellular Carcinoma Immunotherapy. Cancers (Basel). 2020;12(3).

Publisher's note